3D printing of kappa-carrageenan emulsion gels

Kamlow, Michael-Alex; Spyropoulos, Fotios; Mills, Tom

Link to publication on Research at Birmingham portal

3D printing of kappa-carrageenan emulsion gels

Michael-Alex Kamlow*, Fotis Spyropoulos, Tom Mills

School of Chemical Engineering, University of Birmingham, Edgbaston, Birmingham B15 2TT, United Kingdom

ABSTRACT

The interest in personalised food through 3D printing has led to an increased interest in the formulation and production of more complex foodstuffs rather than simple water-based systems. 3% w/w Kappa-carrageenan (κC) emulsion gels were created containing 5–40% w/w sunflower oil (SFO); using two different emulsifiers, Tween 20 (T20) and Whey protein isolate (WPI). Differential scanning calorimetry showed that both T20 and WPI stabilised emulsions had only minor effects on the gelling and melting enthalpies of the κC, and had the same gelling temperatures. All tested formulations were printable under the same printing parameters, provided the feed rate was increased with SFO concentration. Confocal microscopy showed the presence of layering throughout the printed gels and that T20-stabilised emulsion gels had flocculated. Texture profile analysis was used to compare printed and cast $20 \times 20 \times 9.6$ mm cuboids. For cast cuboids, as the SFO concentration increased, the hardness values decreased from 75 N $\pm$ 4 N to 18 N $\pm$ 1.5 N. For printed cuboids the hardness values were constant at 13 N $\pm$ 2 N. Upon compression, printed cuboids delaminated at the areas between the printed layers. Oscillatory rheology showed that cast gels were more resistant to shear strain compared to the printed gels and this was again believed to occur due to delamination between the semi-fused printed layers. This work demonstrates that κC emulsion gels can be 3D printed without a change in their physical performance regardless of SFO concentration up to 40%.

1. Introduction

3D printing (3DP), also known as additive manufacturing, is a technique that has become very widespread in recent years, across a range of sectors. It produces parts in a layer-by-layer manner using digital files that are rendered slice by slice and then uploaded to the printer. At the time of its inception 3DP focused mainly on plastic polymers (Rahim, Abdullah & Md Akil, 2019), metal (Buchanan & Gardner, 2019) and ceramics (Chen, Xie, Chen & Zheng, 2019), but has more recently moved into the exploration of other research areas such as pharmaceuticals (Goyanes, et al., 2017) and food materials such as chocolate (Lanaro, Desselle & Woodruff, 2019) dairy gels (Daffner, Ong, Hanssen, Gras & Mills, 2021), dough (Yang, Zhang, Prakash & Liu, 2018) and various other foodstuffs utilising a range of techniques (Gholamipour-Shirazi, Kamlow, Norton, & Mills, 2020). 3DP's appeal in food production stems from its ability to facilitate the customisation and personalisation of foodstuffs at the point of production, without the use of moulding or tooling (Sun et al., 2015). However, food 3DP still has inherent drawbacks compared to large-scale mass production such as low-throughput, high cost per item fabricated and a narrow range of suitable/printable edible materials that still require research to overcome (Pallottino et al., 2016).

However, one of the biggest challenges in the field of food 3DP is indisputably the complexity of food systems themselves, which often contain several materials in varying ratios, sensory and structural characteristics determined by micro- and nano-structure as well as properties that are ion, temperature and processing dependent (Ubbink, Burbidge & Mezzenga, 2008). Recent studies have focused on the use of hydrocolloid gels (hereafter referred to as hydrogels) for 3DP. Their suitability is owed to the fact that many of them are renewable, biocompatible and are well researched and understood in the food sector. These materials are currently widely used in food and pharmaceuticals by themselves and/or as components in specific formulations (Khalil et al., 2018). Most hydrogel printing studies have focused on the cold-extrusion of already set gels, with no phase transition occurring during the printing process (Gholamipour-Shirazi, Norton & Mills, 2019). This method benefits from not requiring temperature control, higher shape fidelity and the ability to print gels that are not thermally set such as alginate gels. Hot-extrusion 3DP can print highly viscous gels with less difficulty (compared to cold-extrusion), as 'inks' in this case are still in the sol-state (Azam, Zhang, Bhandari & Yang, 2018). Furthermore, longer-term storage of component inks for the hot-extrusion approach would be less of an issue, as many cold-extruded hydrogels exhibit water loss through syneresis (Mizrahi, 2010). However, since hot-extrusion requires melting the materials before use the syneresis that occurs during storage will be far less of an issue. Hot-extrusion 3DP requires hydrogels that rapidly solidify below their gelation temperature (T_{gel}). Past research on the hot-extrusion of 3DP hydrogels has focused on agar (Serizawa et al., 2014), starch (Chen, Xie, Chen & Zheng, 2019) and mixtures of materials (J. Chen, et al., 2019; Liu, Bhandari, Prakash, Mantihal & Zhang, 2019).

One biopolymer receiving particular attention in food 3DP research is kappa-carrageenan (κC). KC is an anionic polysaccharide, containing a sulphate group, extracted from an edible red seaweed called Rhodophyta. When dispersed in water, and in the presence of cationic molecules, κC is able to form a thermally reversible gel, with the greatest

affinity for potassium ions (Hermansson, Eriksson & Jordansson, 1991) Once the dispersion is lowered below the sol-gel temperature, the random κC coils arrange themselves into double helices, which then aggregate to form a polymer network (Norton, Morris & Rees, 1984). KC has many uses in foods as a rheology modifier and thickening agent (Saha & Bhattacharya, 2010). KC has been studied as a biopolymer ink for 3DP in cell printing (Kelder, Bakker, Klein-Nulend & Wismeijer, 2018), hot-extrusion printing as a single biopolymer (Diañez et al., 2019), as a mixed-system (Warner, Norton & Mills, 2019) and in cold-extrusion (Gholamipour-Shirazi et al., 2019). This demonstrates its versatility in 3DP applications owing to its high gel strength and rapid sol-gel transition under the correct conditions.

Since hydrogels are generally formed using approximately 0.1–10% w/v hydrocolloid, small quantities of salts and the rest water, issues exist when it comes to the incorporation of hydrophobic molecules within such constructs. One approach to address this is to create oil-in-water (o/w) emulsions by dispersing oil within a continuous water phase and then allowing this to gel (as it would normally) to create emulsion gels, with the gel matrix acting as the continuous phase. This allows the creation of more complex structures and the incorporation of an oil phase enables straightforward encapsulation of lipophilic molecules within the gel matrix. Emulsion gels have been researched for a long time (Hemker, 1981) and their uses include modification of food texture (Matsumura, Kang, Sakamoto, Motoki & Mori, 1993), delivery of lipophilic drugs (Thakur et al., 2012) and dual delivery of lipo- and hydrophilic drugs (Singla, Saini, Joshi, & Rana, 2012).

Since 3DP of food materials allows for customisation of food structures through ingredient placement (Diaz, Noort & Van Bommel, 2017), it makes sense that the creation of more complex emulsion gels, as opposed to hydrogels should be an area of interest for researchers. This will allow highly customised food items that could still retain the desirable creamy mouth feel of fat based foods, but through use of an emulsion gel could reduce the overall fat content of the food itself (Sala, de Wijk, van de Velde & van Aken, 2008). KC emulsion gels have had some research dedicated to them (Fontes-Candia, Ström, Lopez-Sanchez, López-Rubio & Martínez-Sanz, 2020; Sala et al., 2008), however, to the authors' knowledge there exists little if any literature on the 3DP of κC emulsion gels despite its usefulness as both a food additive and 3DP biopolymer ink. Most studies into 3DP of emulsion gels appear to be based on cold-extrusion techniques (Du, et al., 2021; Liu et al., 2019; Sager, Munk, Hansen, Bredie & Ahrné, 2021), with none assessing whether varying oil concentrations or emulsifiers could affect printability within hot-extrusion 3DP.

This study formulated 3% w/w κC emulsion gels containing a range of sunflower oil concentrations (5–40% w/w). Once simple o/w emulsions were produced, the droplet size was tested via dynamic light scattering and emulsion stability was assessed via zeta-potential measurements. The emulsion was then examined under a light microscope in order to ascertain whether flocculation had occurred or not. After this, emulsion gels were created by dispersing the κC powder into the simple o/w emulsions. The κC emulsion gels were assessed based on the oil concentration and its effects on 3DP κC emulsion gels. Two emulsifiers with different stabilisation mechanisms, were compared since it was hypothesised that the differences in their structures and charge could lead to variation in their interactions with the gel structure. They were evaluated by micro differential scanning calorimetry (μDSC) in order to ascertain their T_{gel} and melting temperature (T_{melt}), as well as their gelling and melting enthalpies. Following this, 3D printing took place, testing several parameters to optimise print quality. After suitable and consistent 3DP gels could be fabricated the gels' mechanical properties were ascertained through texture profile analysis (TPA) and oscillatory rheology comparing printed gels to cast gels over a range of oil concentrations. Finally, the emulsion gels were imaged using confocal laser scanning microscopy (CLSM) in order to visualise any difference between 3DP and cast emulsion gels as well as emulsion gels stabilised by T20 and WPI.

2. Materials and methods

2.1. Materials

κC and T20 and were purchased from Sigma-Aldrich (UK). Nile red was purchased from Fischer Scientific (UK). WPI was obtained from Sachsenmilch Milk & Whey Ingredients (Sachsenmilch Leppersdorf GmbH, Wachau, Germany). According to the manufacturer it contained 93.74% w/w protein in dry matter, 0.23% w/w fat, 0.61% w/w lactose and 3.16% w/w ash. Sunflower oil was purchased from the supermarket Spar (UK). Milli-Q water was used (Elix® 5 distillation apparatus, Millipore®, USA) for sample preparation. All materials were used as received with no further modification or purification.

2.2. Preparation of κC solutions containing emulsifiers

κC solutions containing the emulsifiers were produced to be used as 0% w/w sunflower oil gels. This was to ensure any changes observed were caused by the presence of the sunflower oil and not just the emulsifying agent. κC solutions containing T20 were produced by adding 3% w/w κC to 192 mL of deionised water which had been placed on top of a hotplate-stirrer set to 80 °C. A magnetic stir bar was used to aid with dispersion of the κC into the water. This was left to stir for two hours. After the κC had dispersed 1% w/w T20 was added to the heated κC solution and this was stirred at a lower speed for another 30 min following the method set out in previous studies (Fenton, Kanyuck, Mills & Pelan, 2021). κC solutions containing WPI were produced by first dispersing 2% w/w WPI in deionised water and stirring at 40 °C for five hours. This WPI stock solution was then stored in the fridge overnight to allow for full hydration. 100 g of the 2% w/w WPI solution was then diluted by adding to 94 g of deionised water. This was then heated and the κC powder dispersed as above. This gave a final solution of 1% w/w WPI and 3% w/w κC.

2.3. Emulsion preparation

Simple emulsions containing no κC were produced for particle size analysis and zeta-potential measurements. This was because these tests cannot be carried out in a straightforward manner on gelled samples. Sunflower O/W emulsions stabilised with T20 were produced by first measuring out the required amount of water and then adding 1% w/w of T20 to the water. This was stirred gently with a magnetic stirrer for 10 min. Then, the required percentage of oil was added and premixed on a Silverson L5M for 3 min at 6000 rpm with a fine emulsor screen. The formed pre-emulsion was then passed through a high-pressure homogeniser at 25 bar. O/W emulsions stabilised with WPI were made by using the WPI stock solution described in 2.2, which was added to the required amount of oil and processed as described for the T20 emulsions.

2.4. κC-Emulsion solution preparation

T20 and WPI stabilised O/W emulsions (as described in Section 2.3) were used for the preparation of κC-emulsion solutions. Emulsions were first placed on a hotplate-stirrer set to 80 °C for 30 min. Then κC was added and left to stir for two hours to ensure that all κC had been dispersed. Because of the varying amount of oil (dispersed) phase in the emulsions, the amount of κC added to each system was kept constant at 3% w/w with reference to (in each case) the aqueous (continuous) phase fraction. In this way the amount of κC in the aqueous phase of all O/W emulsions (regardless of their oil content) was the same. The 3% w/w κC concentration was chosen as this was previously reported to give optimal printing outcomes (Kamlow, Vadodaria, Gholamipour-Shirazi, Spyropoulos & Mills, 2021). Finally, O/W emulsion gels were formed by cooling the systems, either via 3D printing as described in Section 2.8 or casting in moulds as described in Section 2.9.

2.5. Particle size analysis

The emulsion droplet size was obtained using a Malvern Mastersizer MS 2000 (Malvern Panalytical, UK), utilising a Hydro SM manual small volume sample dispersion unit. The values for refractive index were input into the software and were 1.33 for water and 1.467 for the sunflower oil. The sample was dispersed in distilled water at 1300 rpm until an obscuration value of 4.2–4.6% was achieved. This gave values for the volume mean droplet diameter ($d_{4,3}$) and unless stated otherwise, droplet size refers to this parameter. Samples were prepared and tested in triplicate and droplet size values were the average of at least three measurements. Droplet size values were obtained immediately after preparation.

2.6. Zeta-potential measurement

The zeta potential (ζ-potential) was determined using a Zetasizer (Malvern Panalytical, UK) in order to assess the stability of the emulsions created. Samples were diluted 100 times with deionised water (Wu et al., 2016). This was to reduce the absorbance of laser light and multiple scattering. All ζ-potential measurements were carried out at room temperature. Samples were prepared and tested in triplicate, and the zeta-potential values were the average of at least three measurements.

2.7. Micro differential scanning calorimetry

Micro Differential Scanning Calorimetry (μDSC) was carried out using a Seteram MicroDSC3 evo (Seteram, France). Experiments were performed over a range of temperatures for the hydrogels and the emulsion gels following the same procedure as that previously described by (Kamlow et al., 2021). The tested temperature range was 0–70 °C, and tests were carried out at a scan rate of 1 °C per minute for both cooling and heating. The samples were first cooled to 0 °C and held for 60 min and then heated to 70 °C and cooled back down to 0 °C. This was repeated three times per sample. This temperature range was chosen since all thermal transitions occurred within this range. Each different formulation was tested in triplicate in this manner, giving a total of nine cooling and heating curves per formulation.

2.8. 3D printing

The 3D printer was supplied by the Institute of Food Science and Biotechnology at the University of Hohenheim (Germany). It is a Fabbster 3D printer that has been modified in order to handle a liquid feed. This modification involved retrofitting several hoses onto the printer containing inner pipes where the material flows through and a surrounding water environment in order to maintain the temperature of the gel to keep it in the sol state. These were connected to two water baths. These pipes carry water to and from the printer by counter-flow. One set is responsible for the gel solution being kept above its T_{gel} from the syringe to the nozzle (1. and 2. in Fig. 1A) and the other set ensures that the temperature within the final length of pipe including the nozzle can be controlled (3. and 4. in Fig. 1A). This enabled maintenance of the sol state, which would then enable the sol-gel transition to occur *in situ* as with previous studies (Kamlow et al., 2021; Warner et al., 2019). This prevented any pre-gelation before the feed material reached the nozzle. To further control the rate at which the phase transition could occur, there was a heated bed, with a removable section (6. and 7. in Fig. 1A). The temperature was controlled by a third water bath connected by insulated pipes (5. in Fig. 1A). The syringe pump (8. in Fig. 1A) was equipped with a 60 mL syringe wrapped with a heating pad (9. and 10. in Fig. 1A). This prevented the feed material in the syringe from undergoing premature gelation. The heating pad was powered with a computer power supply unit and controlled with an Arduino Uno, to control the heating pad temperature (11. and 12. in Fig. 1A). Several

temperature probes were placed at various points on the printer and monitored with a data logger (13 in Fig. 1A). The printer is controlled by a laptop connected to a controller (14. and 15. in Fig. 1A). This allows to the printer to move in the XYZ axis via the arms and motors that form the frame of the printer (16. and 17. in Fig. 1A). Fig. 1B shows the nozzle itself. The outer pipe (4. in Fig. 1B) is made from copper and inside contains a smaller brass pipe where the feed material flows through. It is held in place using a stainless-steel mount made by the technical workshop of the University of Hohenheim. This is surrounded by water flowing in a counter current to the flow of the feed material. There are two 3D printed parts (3. and 7. in Fig. 1B) which allow for connection of the pipes and form the nozzle from which the gels are extruded onto the printing bed. Thermocouples to monitor temperature of the feed material were placed at the top and the bottom of the copper pipe (2. and 6. in Fig. 1B). Several parameters for the printing itself were tested. Some were controlled by the printer software (Netfabb for Fabbster, Fabbster, Germany), such as layer height, print speed and fill spacing. These parameters have been shown to have a major effect on print fidelity in food systems before (Severini, Derossi, Ricci, Caporizzi & Fiore, 2018; Yang, Zhang, Bhandari & Liu, 2018). The nature of this printer's operation meant that the syringe driver rate was responsible for the amount of material extruded and so this had to be tested and controlled. Print success was judged according to weight consistency and final shape fidelity (Chimene, Lennox, Kaunas & Gaharwar, 2016).

2.9. Production of moulds for casting

A cuboid shaped mould was produced by stereolithography 3D printing using a form 2 3D printer (Formlabs, USA). The mould was designed by CAD and uploaded to the software, this was then sliced and sent to the printer digitally to print. This mould would allow the production of hydrogel and emulsion gel cuboids with dimensions of $20 \times 20 \times 9.6$ mm by casting. These were then used for comparative mechanical testing as a control, cast sample to compare to the 3D printed cuboids produced in 2.8.

2.10. Texture profile analysis

Texture profile analysis (TPA) was carried out using a TA XT plus Texture Analyser as described in previous studies (Kamlow et al., 2021). Printed and cast cuboids of dimensions $20 \times 20 \times 9.6$ mm were tested; the cast cuboids were given 3 min 30 s to set, mimicking the time taken to print their respective counterparts. Tests were carried out using a P/40 cylindrical aluminium probe set to a constant speed of 1 mm/s, alongside a 30 kg load cell and 3 g of trigger force. Through compression testing, data for hardness and Young's modulus was acquired for printed and cast cuboid. Hardness is calculated from the peak force during the initial compression cycle, while Young's modulus is the stiffness of the material calculated through the stress/strain relationship of the material at low strains (Jones, Woolfson & Brown, 1997). All tests were carried out in triplicate, and the hardness and Young's modulus values were the average of at least three measurements.

2.11. Rheological testing

Rheological tests were performed using a modular compact rheometer 302 (Anton Paar, Austria) using a parallel 25 mm serrated plate. For cast gels, the rheometer was heated to 60 °C and then the sample was loaded on. Then a working gap of 1mm was used and the excess trimmed off. The temperature was then lowered to 20 °C and each sample was left to equilibrate for ten minutes. Then, amplitude sweeps were performed at a fixed frequency of 1 Hz and the strain amplitude was varied from 0.1 to 10%. This matched previous studies where gel brittleness made testing above that level of strain unnecessary (Jong, 2020; Loizou et al., 2006). For 3DP samples a disc 1 mm high and 30 mm in diameter was printed. Owing to the inability to reliably remove the single layer disc
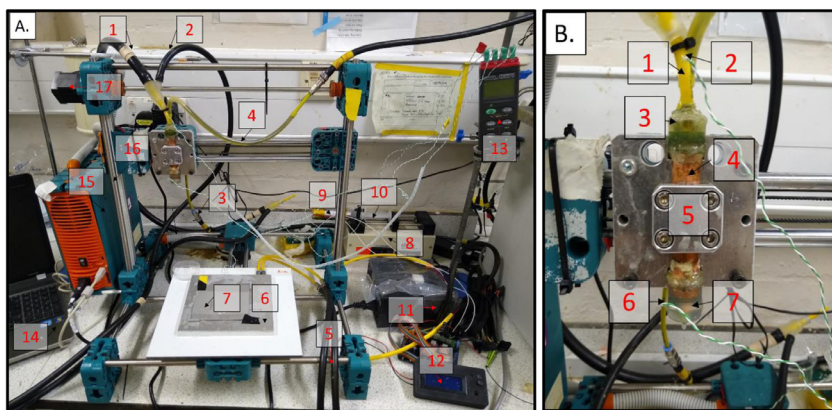
Fig. 1. Schematic of the retrofitted Fabbster printer (**A**) including (1) Jacketed pipe from the syringe to the nozzle, (2) Jacketed pipe from the nozzle to the water bath, (3) Jacketed pipe from a water bath to the bottom of the nozzle, (4) Pipe from the top of the nozzle to the water bath, (5) Jacketed pipes to and from a water bath to the temperature controlled bed, (6) Temperature controlled printing bed (7) Removable section of the printing bed (8) Syringe driver, (9) Heating jacket, 10) 60 mL syringe, 11) Power supply unit, (12) Controller for heating jacket, (13) Data logger, 14) Laptop to control printer, (15) Controller unit for the printer, (16) Support rods for the printer, (17) Support rods and motor for the printer. (**B**) Schematic of the printer nozzle including (1) Feed pipe into the nozzle, (2) Thermocouple to monitor temperature of feed material as it enters the nozzle, (3) 3D printed part to connect feed pipe to the copper pipe, (4) Copper outer pipe containing brass inner pipe, (5) Bracket to hold copper pipe in place, (6) Thermocouple to monitor temperature of feed material as it enters the die, (7) 3D Printed nozzle. The printer was connected to and controlled by a computer running Netfabb for Fabbster software.

from the printing bed, the printing bed was removed and placed on the rheometer. The printing bed was 1 mm thick, so the rheometer was set to use a 2.015 mm working gap owing to the placement of foil on the bottom plate of the rheometer to prevent it being scratched by the printing bed. This allowed for reliable data to be obtained and the printed sample was given eight minutes to equilibrate at 20 °C. This allowed for the 40 s print time and the approximate one minute needed to transfer the print bed containing the sample to the rheometer. This gave data for the linear viscoelastic region (LVER), storage modulus (G') and loss modulus (G'') as the function of shear strain. Samples were prepared and tested in triplicate, and the values were the average of at least three measurements.

2.12. Confocal laser scanning microscopy

Emulsion gel samples were produced for CLSM by the addition of nile red to the oil phase before emulsification. A Leica DM2500 confocal microscope (Leica®, CH) was used for the imaging. Three different objective lenses were used 10 times, 40 times and 63 times, with immersion oil being used for the 63 times objective. A 532 nm laser at 100% intensity was used to excite the dye and emissions at the range of 550–700 nm wavelength were detected for imaging in line with previous studies (Vadodaria, He, Mills & Wildman, 2020). Stained, gelled samples were placed onto glass slides. For 3DP samples discs 500 μm high and 18 mm in diameter were printed directly onto a glass slide and a glass cover slip was placed over the top.

2.13. Statistics

The average droplet size, hardness and Young's modulus values were compared using the two-sample T-test in the Analysis ToolPack for Microsoft Excel. Confidence levels were set at 95%. Therefore, if $P < 0.05$, the two sets of data have different means, otherwise the two means have no significant difference.

3. Results and discussion

3.1. Droplet size analysis and zeta-potential measurements

The droplet sizes of O/W emulsions stabilised by either T20 or WPI and containing varying amounts of sunflower oil (dispersed phase) were measured; the droplet size data is presented in Fig. 2A, with the distributions presented in Fig. 2B and C. To minimise the risk of phase inversion in the system, the sunflower oil content in the emulsions was kept below 50%. The emulsifier concentration (T20 or WPI) was fixed at 1% w/w which was sufficient to enable emulsion stabilisation.

Statistical analysis showed no significant difference between the SFO concentrations' effect on droplet sizes. Another point of note is that increasing the amount of dispersed phase can have a negative impact on the longer term stability of emulsions containing emulsifier concentrations used in this study (Dapčević Hadnađev, Dokić, Krstonošić & Hadnađev, 2013). However, this was not an issue in this case as shortly after the formation of these emulsions they were to be 3D printed into κC-emulsion gels. The data in Fig. 2A also shows that on average the emulsions stabilised by T20 had smaller droplet sizes than those stabilised by WPI, ranging from around 11–13 μm to 18–22 μm, respectively, which was a statistically significant difference. This is due to low molecular weight surfactants (LMWS), owing to their smaller size, being able to position themselves at the interface quicker than proteins, which take longer to orientate and unfold themselves at the interface (Kenta et al., 2013). Furthermore, LMWS such as T20 decrease interfacial tension more than proteins, and this further enhances droplet breakup (Beverung, Radke & Blanch, 1999).

After producing the emulsions, they were then tested for their ζ-potential to assess the surface charge on the oil droplets. The results for the ζ-potential measurements are shown in Fig. 3. The ζ-potential values for the emulsions stabilised by T20, show that T20 does not carry much surface charge giving values of -6mV to -8mV. This is typical for non-ionic emulsifiers, since they do not rely on surface charge to stabilise emulsions but instead do it through steric repulsion (Teo et al., 2016). However, even though non-ionic surfactants would not expect to present with any surface charge, it has been shown before that ionised surface-active impurities like free fatty acids can lead to some charge being detectable in emulsions stabilised by non-ionic surfactants (Wu, Yan, Chen & He, 2017). Whereas because the emulsions were all at neutral pH, the emulsions stabilised by WPI had a negative charge. This is because neutral pH is above the isoelectric point of the WPI which, is around 4–6 (Chanamai & McClements, 2002), giving the protein molecules a negative surface charge. This explains why the WPI emulsions had ζ-potential values of around -34 mv to -37mv with the small differences being within the error values of each other.

3.2. Pre-printing μDSC analysis of emulsion gels

It was first important to establish the thermal characteristics of the κC gels, as this is necessary in designing printable formulations for hot-extrusion printing. After they were established, then κC emulsion gels could be characterised and assessed for their suitability in 3DP. Previous studies reported that increasing the concentration of oil led to an increase in gel strength, T_{gel} and T_{melt} values. However, this was due to the total concentration of κC remaining constant in the formulations, leading to an effective increase in κC concentration in the water phase as the oil concentration increased (Fontes-Candia et al., 2020). So, it
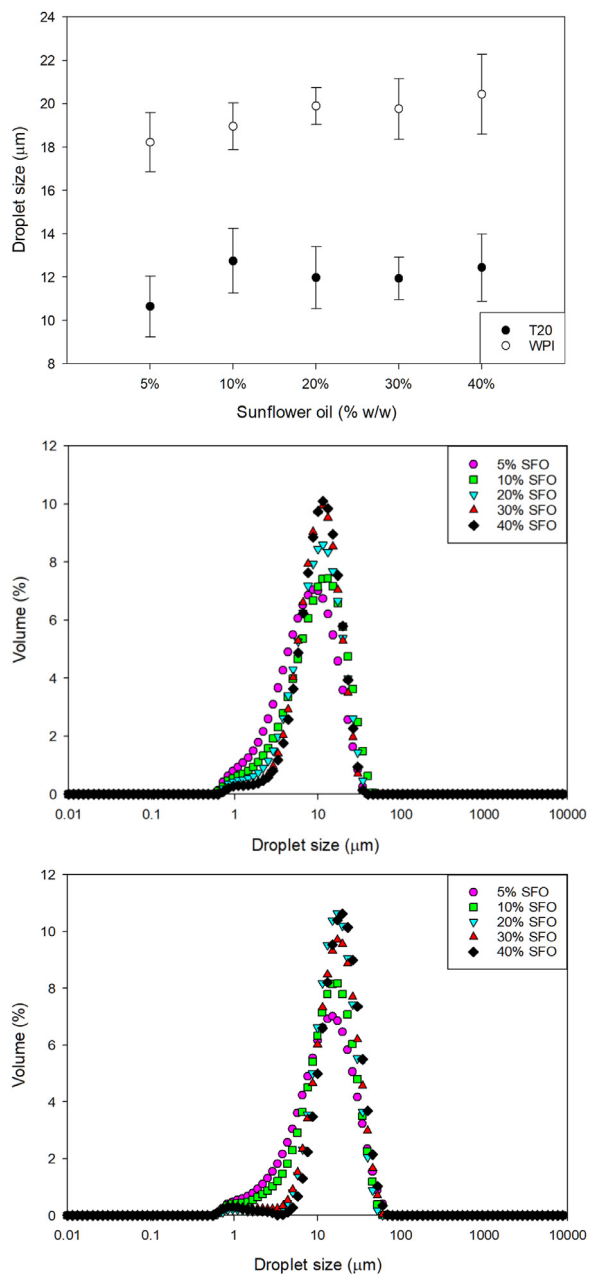
Fig. 3. ζ-potential of O/W emulsions stabilised by either T20 or WPI as a function of sunflower oil (dispersed phase) content.

Fig. 2. (A) Comparison of the average droplet size of emulsions produced using a range of sunflower oil concentrations and 1% T20 or 1% WPI, (B) Droplet size distribution for T20 stabilised emulsions and (C) Droplet size distribution for WPI stabilised emulsions.

was important to assess the effects of varying oil concentration on the T_{gel} and T_{melt} of κC-emulsion gels while maintaining the same concentration of κC in the water phase. The sol-gel transition temperatures of the emulsion gel systems were determined using a micro differential scanning calorimeter (Iijima, Hatakeyama, Takahashi & Hatakeyama, 2007; Snoeren & Payens, 1976; Williams, Clegg, Langdon, Nishinari & Piculell, 1993). The results for mean T_{gel} and T_{melt} for 3% κC emulsion gels with 0, 5, 10, 20, 30 and 40% w/w sunflower oil are shown in Fig. 4A. Gelling and melting enthalpies for the assessed systems are found in Fig. 4B. Fig. 5A and B show the DSC micrographs for gelation and melting, respectively.

Fig. 4A shows that if the concentration of κC is kept constant in the water phase of emulsion gels, the T_{gel} and T_{melt} of the systems stay approximately constant. This was important, because if the con-
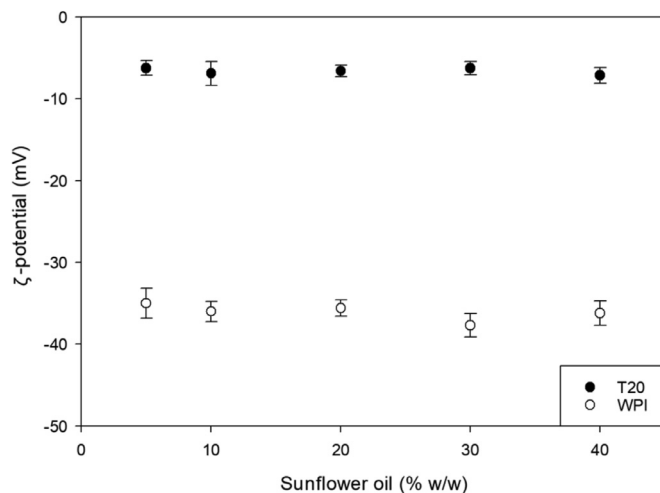
centration of the κC was not adjusted to remain at 3% w/w in the water phase, then the effective concentration would have kept increasing and each concentration of SFO would have required different printing parameters. Furthermore, as far as the data for T_{gel} in Fig. 4A shows, both emulsifiers had the same T_{gel} values, of 36-37 °C. This meant that they could be printed at the same temperatures. However, the T_{melt} data showed that there was a statistically significant disparity of 1-2 °C between the emulsion gels stabilised by T20 and those stabilised by WPI. As stated in 2.1 the WPI was assessed to contain 3.16% ash. Milk-based ash is known to contain cations such as potassium and calcium (Aaltonen, Kytö, Ylisjunttila-Huusko & Outinen, 2020). Cations are known to cause the reinforcement of κC gel networks (Hermansson et al., 1991) and so would cause an increase in the melting temperature. However, another explanation could have been that the WPI was interacting with the κC. Though this was unlikely as the WPI was at pH 7, which is above its isoelectric point and therefore its overall net charge would be negative. Since κC in anionic, it cannot electrostatically interact with another anionic molecule such as negatively charged WPI. However, the enthalpy data in Fig. 4B suggests that there was no interaction between WPI and κC as the enthalpy values for both types of emulsion gels are approximately equal. This implies that there were no new bonds being formed, which would indicate that the differences seen in Fig. 4A were down to the presence of cations with the WPI, reinforcing the κC gel network.

The data in Fig. 4B shows that once normalised to a constant κC concentration, the gelling and melting enthalpies remain practically consistent, with a slight decrease seen in the gelling enthalpies. This shows that addition of the oil has little, if any impact on the gel network itself. This is in contrast with what has been observed with emulsion gels before (Dun et al., 2020; Liu et al., 2019). These studies did not appear to normalise their data to κC concentration per 100 g of water, which since adding more oil would lead to less κC per 100 g, led to an apparent decrease in enthalpy values. Since the emulsion droplets were coated in either a non-ionic surfactant (T20) or a negatively charged protein they were non-interacting filler particles. Therefore they did not enhance the gel network, unlike an interacting filler (Mcclements, Monahan & Kinsella, 1993)

3.3. Hydrogel and emulsion gel printing

All printed emulsion gel samples contained 3% w/w κC in the water phase, 1% w/w emulsifier and between 0 and 40% w/w sunflower oil. Since the μDSC data had shown the emulsion gels to have T_{gel} values of 36-37 °C, the temperature probe (16. in Fig. 1B) was used to monitor the
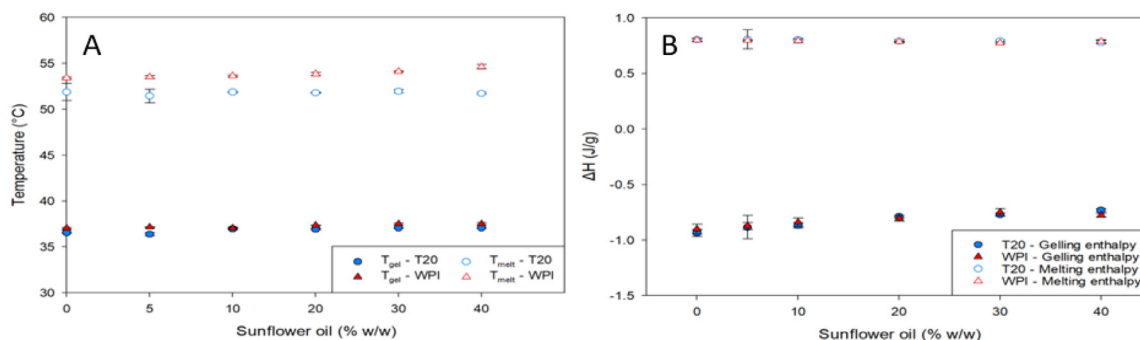
Fig. 4. DSC data for (A) the average thermal transition temperatures (T_{gel} and T_{melt}) and (B) the gelling and melting enthalpies of κC emulsion gels with varying sunflower oil concentrations, stabilised by Tween 20 and WPI.
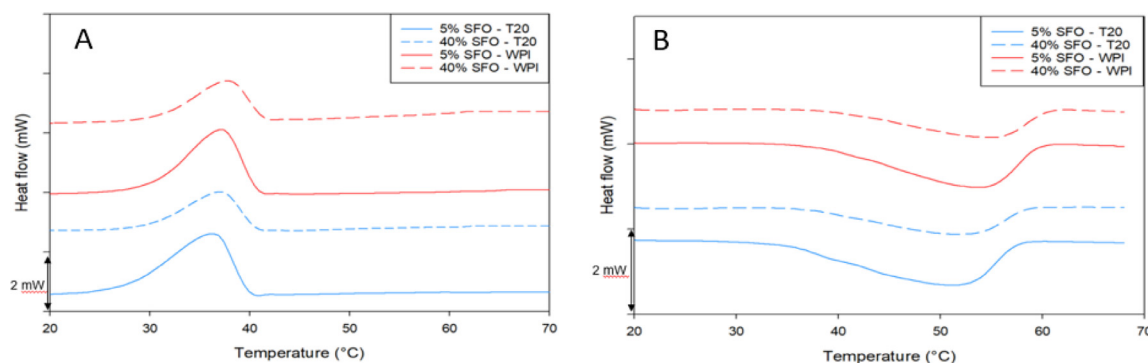

Fig. 5. DSC micrograph data for (A) the gelling and (B) melting enthalpies of κC emulsion gels, stabilised by Tween 20 and whey protein isolate, with 5% and 40% w/w concentrations of sunflower oil.

feed material and ensure that it would be exiting the nozzle around 9–11 °C higher than the gelling temperature. This has been shown to give optimal printing in previous studies (Warner et al., 2019). The printing temperature was determined indirectly by the water baths attached to the printer, hence why the temperature probes were used to monitor the feed material temperature. The parameters tested for the 3D printing are shown in Table 1.

Apart from the parameters defined in Table 1, other parameters which were variable existed. These were layer height, nozzle size and nozzle height. The layer height was left as 1.2mm because this was suggested in our previous study (Kamlow et al., 2021) to be the optimal layer height for κC hydrogels; and this was confirmed to hold true in this study as well. The nozzle for the printer (7. in Fig. 1B) was a 3DP part and had to be sealed with glue and silicone to prevent water leakage. Therefore, it was not practical to test and change various nozzle sizes, and therefore the same optimal nozzle size (20G/0.8 mm) from the previous work was again used as the standard. Finally, the nozzle height was kept at a constant at 0.5 mm as these yielded prints with no issues and, unless stated otherwise, was the height used for all prints. The print settings from Table 1 that gave the best shape fidelity and reproducibility were: S_R of 0.7 mL/min, T_{PB} of 35°C, V_P of 30 mm/s, a Fill of 1.25 mm, T_{HWB} of 72 °C and T_{NWB} of 72 °C

While the above settings were viable for 0% w/w SFO and 5% w/w SFO, voids were seen in higher oil concentrations under the same printing conditions as seen in Fig. 6 Table 1. These failed prints were believed to be due to the increasing concentration of SFO in the κC-emulsion solutions. This led to an increase in the viscosity of the κC-emulsion solution, since the oil droplets are more densely packed (Pal & Rhodes, 1989). This meant that maintaining the S_R for higher oil concentrations led to a decrease in the amount of feed material being extruded. This problem can be overcome by increasing the extrusion rate to prevent the formation of voids (Dick, Bhandari & Prakash, 2019). The nature of the printing setup used meant that this was achieved through increasing the
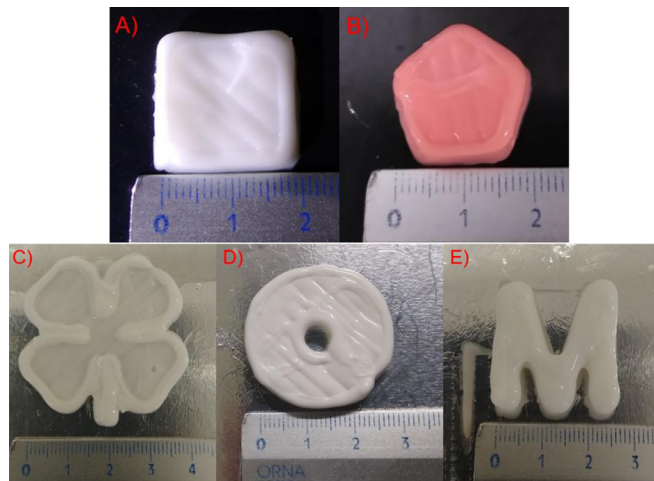

Fig. 6. Examples of successful prints (A) 5% SFO 20 × 20 × 9.6 mm cuboid, (B) Pentagon containing 10% SFO and 0.4% red food colouring, (C) Four leaf clover printed with 20% SFO, (D) Torus printed with 30% SFO and (E) 'M' printed with 40% SFO.

S_R. The S_R values for acquiring high quality print outcomes are shown in Table 2. Once the optimal syringe driver rates for each sunflower oil concentration were determined it was possible to print complex geometries using any of the concentrations tested. Various successful prints from the printer are shown in Fig. 6.

3.4. Emulsion gel imaging

While the non-printed samples could be positioned onto a hot microscope slide and then a cover slip placed over them before they gelled,

Table 1

A table showing the different parameters tested in the gel 3D printing process as well as failed prints showing a cube that the nozzle had dragged through, an over-extruded cube with excess material and an under-extruded cube with voids.

S_R (mL/min)	T_{PB} (°C)	v_p (mm/s)	Fill (mm)	T_{HWB} (°C)	T_{NWB} (°C)	3D Outcome and Comments
1.2	20	20	0.5	60	58	Over extruded – very poor shape fidelity
0.8	20	20	0.5	60	58	Over extruded – shape recognisable
0.6	20	20	0.5	60	58	Under extruded – voids in the print
0.7	20	20	0.5	60	58	No voids but poor bottom layer ruined print
0.7	40	20	0.5	60	58	Print bed too hot, shape couldn't be built up
0.7	35	20	0.5	60	58	Shape fidelity acceptable – layers not fused
0.7	35	20	0.5	66	66	Nozzle dragged through printed material
0.65	35	20	0.5	66	66	Nozzle dragged through printed material
0.65	35	20	0.75	66	66	First few layers fine, but top layers poor
0.65	35	20	1	66	66	Fidelity good, but voids present
0.7	35	20	1.25	66	66	Shape resembled CAD file, but layers still not well fused
0.7	35	20	1.25	72	72	Shape resembled CAD file; layers do not separate when handling
0.7	35	20	1.25	80	80	Shape resembled CAD file; layers do not separate upon handling – however, part of the printer deformed and broke at this temperature; so, it was not used any further
0.7	35	25	1.25	72	72	Shape resembled CAD file, even at higher speed; layers do not separate when handling
0.7	35	30	1.25	72	72	Shape resembled CAD file, even at higher speed; layers do not separate when handling
0.7	35	35	1.25	72	72	Shape fidelity less repeatable – speed to be kept at 30 mm/s

SR: Syringe driver rate (mL/min)
TPB: Printer bed temperature (°C)
vp: Print speed (mm/s)
Fill: Fill space (mm)
THWB: Water bath temperature on the feed pipes (°C)
TNWB: Water bath temperature on the nozzle (°C)

Table 2

Table showing variances required in syringe driver rate in order to achieve successful printing based on SFO concentration.

Sunflower oil concentration (% w/w)	Syringe driver rate (mL/min)
0	0.7
5	0.7
10	0.72
20	0.76
30	0.80
40	0.84

this was not feasible for the 3DP samples. The printer was unable to print a thin enough layer for light to pass through the gel. Furthermore, compression of samples with a cover slip has been shown to be problematic in terms of yielding a representative sample (Gibson & Lanni, 1991). Therefore, CLSM was used for both cast and 3DP emulsion gels; the sunflower oil dispersed phases of both printed and cast gels were stained with nile red. Confocal images in Fig. 8 show the distribution of oil droplets in both cast and 3DP samples for emulsion gels stabilised by either T20 or WPI.

Representative confocal images show the distribution of the SFO droplets within the set κC matrices. As evidenced by Fig. 8A, κC emulsion gels stabilised by T20 exhibited clear signs of flocculation between oil droplets. Whereas Fig. 8B shows that the emulsion gels stabilised by WPI are well distributed throughout the gel network. The addition of low concentrations of κC has been shown to cause extensive flocculation of emulsions by depletion effects. More specifically, when the κC is able to electrostatically interact with the molecules stabilising the emulsion droplets, bridging flocculation can take place (Gu, Decker & McClements, 2005), such as when a protein below its isoelectric point is present. Otherwise, when the κC can't complex with the emulsifying agent, depletion flocculation is observed (Singh, Tamehana, Hemar & Munro, 2003).
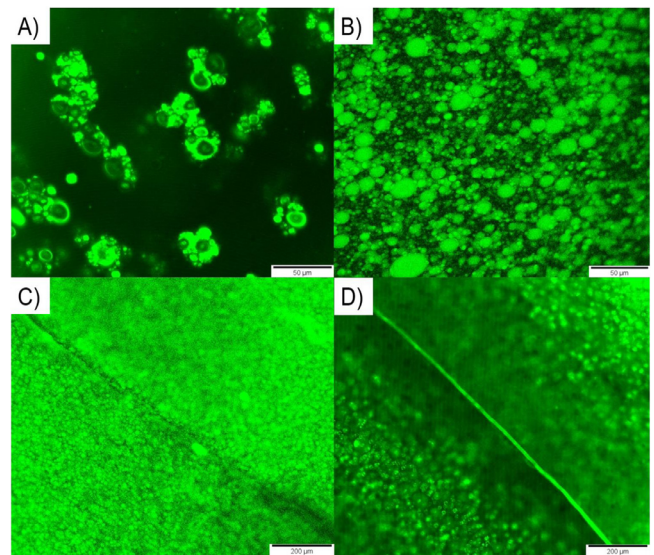

Fig. 7. Confocal microscopy images of (A) Cast κC emulsion gel stabilised by T20, (B) Cast κC emulsion gel stabilised by WPI, (C) 3DP κC emulsion gel stabilised by T20 and (D) 3DP κC emulsion gel stabilised by WPI. The lines observed in (C) and (D) are lines of the printing observed at the same height. For more information see full text.

During the emulsion gel production, as the κC powder was dispersed, its concentration increased quickly, but the low concentrations that can cause depletion flocculation were still present for a certain time leading to flocculation effects. However, emulsions stabilised by T20, were created separately to κC hydrogel solutions and when combined together, immediately flocculated which means that at any κC concentration up to 3% w/w in the water phase, flocculation is observed in the emulsion gel
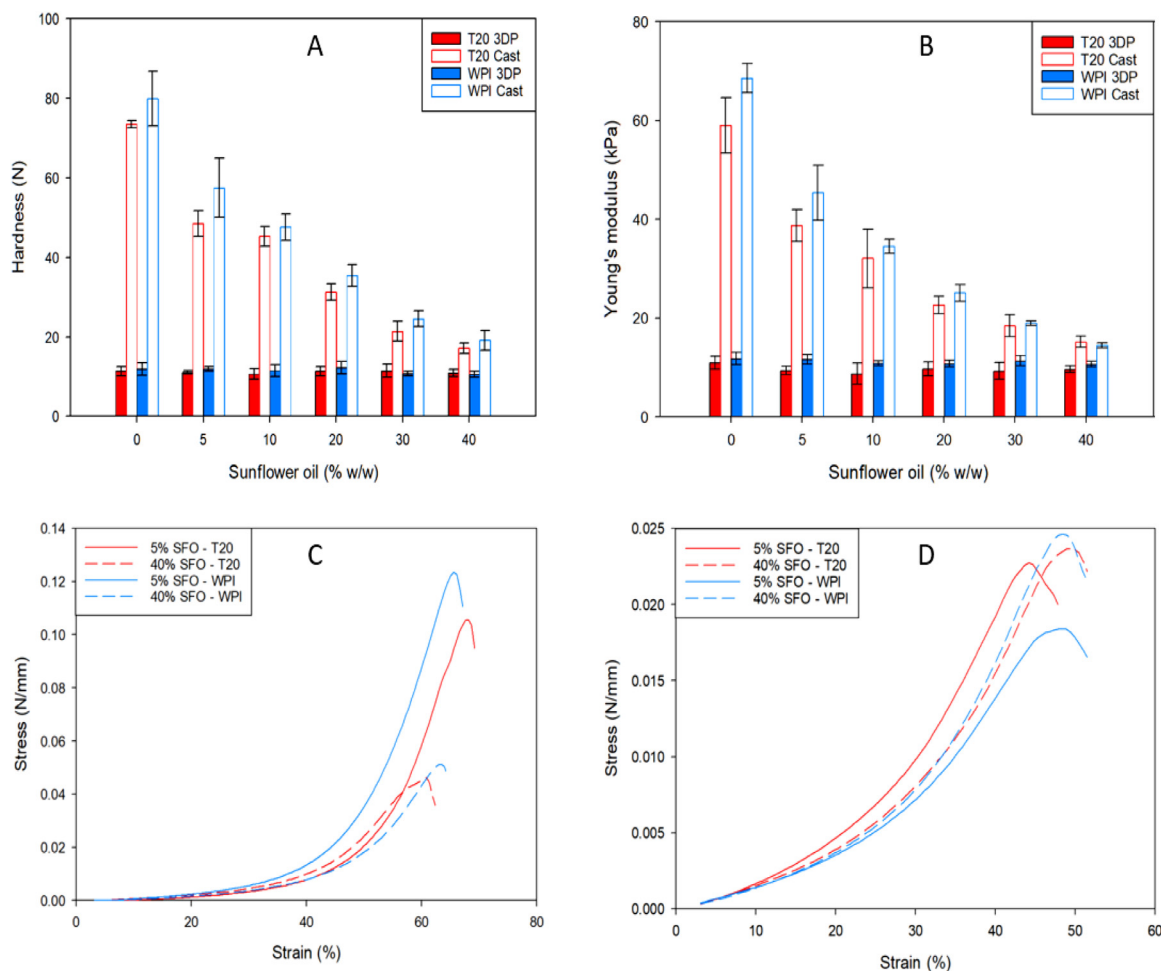
Fig. 8. Hardness (A) and Young's modulus (B) of the printed and cast κC emulsion gel cuboids containing emulsions stabilised by T20 and WPI and stress-strain curves of cast (C) and 3DP (D) cuboids.

systems. However, the WPI stabilised emulsion gels were still dispersed throughout the gel networks. It is believed that the thicker viscoelastic layer formed at the interface by the WPI particles compared to the T20 (Wilde, Mackie, Husband, Gunning & Morris, 2004) before the addition of the κC gave these emulsions greater resistance to the depletion effects. Then, as the viscosity of the continuous phase increased with the κC (Iglauer, Wu, Shuler, Tang & Goddard III, 2011) this slowed down the flocculation to a large extent, leading to presentation of dispersed emulsion gels. Another factor, shown in Fig. 3 is the differences in ζ-potential between the T20 and WPI stabilised emulsion gels. Since WPI has a far higher level of negative charge on the oil droplets, they will repel each other more than the uncharged T20 droplets. This gives it more resistance to the flocculation effects.

Fig. 8C and D highlight the differences in the bulk structures produced by 3DP compared to those of traditional cast gels. The distinct layering that exists throughout the emulsion gels in Fig. 8C and D, due to printing, is absent from the continuous networks seen in Fig. 8A and B. It is created by the discontinuous network produced by the 3DP process, specifically the movement of the nozzle in the x- and y-axes. Variances in the planes of focus around the printed lines, indicate there are differences in depth around the lines themselves. This can be seen by the inability to focus and visualise all the oil droplets in the 3DP confocal images. This shows how the 3DP process gives a different surface to traditional casting. This can be imaged using a z-stack in which several planes of focus are put into a composite video or image. One such video of Fig. 8D can be found in the supplementary information in this paper,

showing a composite z-stack video allowing all the oil droplets to be sequentially visualised.

3.5. Post-printing texture profile analysis

Texture profile analysis of gels is an established technique for testing the performance of their microstructure and whether this affects functionality. In the past, this has generally focused on the release of molecules, such as flavour (Boland, Delahunty & van Ruth, 2006) and therapeutic molecules (Özcan et al., 2009). 3D printing is known to fabricate structures with differing internal structure to their casted equivalents (Padzi, Bazin & Muhamad, 2017) and previous works have demonstrated this to be true for hydrogels (Kamlow et al., 2021). While there have been studies assessing the performance of emulsion gels by TPA (Sala, Van Aken, Stuart & Van De Velde, 2007; Sala, van Vliet, Cohen Stuart, Aken & van de Velde, 2009), there exists little literature examining TPA of 3DP emulsion gels. First typical stress/strain curves were obtained and these were analysed in order to calculate hardness and Young's modulus values of 3DP and cast cuboids containing varying concentrations of SFO.

The data from the TPA shows that as the concentration of the SFO increases, a decrease in both the hardness and Young's modulus values are observed for both types of cast emulsion gels. This is a known phenomenon whereby non-interacting filler particles disrupt the formation of the gel network, leading to weaker gels (Mcclements et al., 1993).
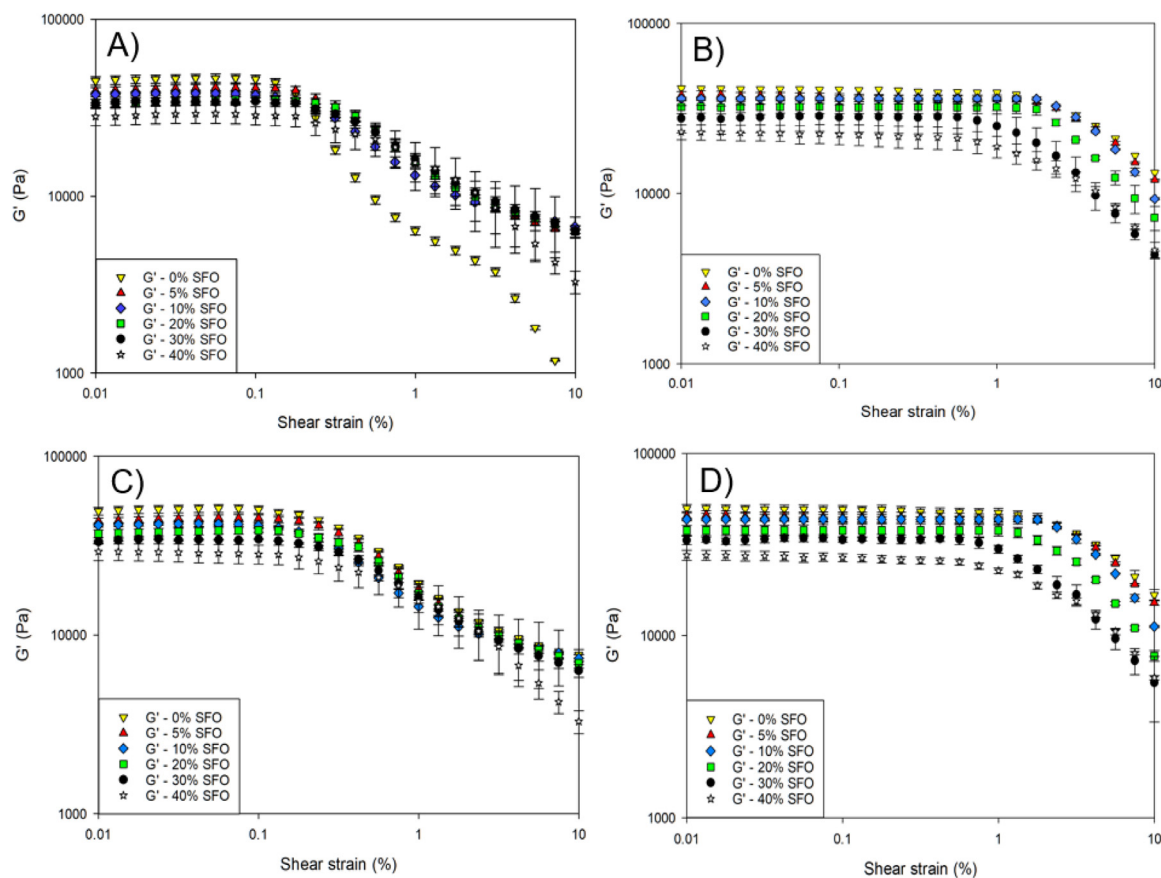
Fig. 9. Amplitude sweep results for κC emulsion gels stabilised by T20 (A) 3DP and (B) cast, as well as κC emulsion gels stabilised by WPI (C) 3DP and (D) cast.

Statistical analysis of the TPA data, again showed that there were no significant differences between the emulsion gels stabilised by WPI and T20 for hardness or Young's modulus. This was despite the salts present with the WPI reinforcing the κC network slightly as shown in Fig. 4 as well as the flocculation of the T20 emulsion gels leading to larger effective droplet sizes within the network, which has been shown to weaken emulsion gels before (Kim, Gohtani, Matsuno & Yamano, 1999). Another study into the large deformation properties of κC gels containing emulsions stabilised by WPI or T20 also found no significant difference between their Young's modulus, fracture stress and fracture strain values (Sala et al., 2007). However, this study used a κC concentration of 0.75% w/w compared to the 3% w/w tested here. Furthermore, the oil droplets in the tested gels were around 1 μm compared to the 8–14 μm droplets in the emulsion gels tested in this study. This shows that there still exists a conflict within the literature, owing to the various interlinked parameters that impact on the structural response of emulsion gels.

However, for the 3DP emulsion gels, the same approximate values for hardness and Young's modulus were observed regardless of oil concentration, with the values being constantly lower than those of the cast cuboids and unaffected by the increasing SFO concentration. A recent study by Kamlow et al. (2021) demonstrated that compression of 3DP gels leads to delamination rather than fracture, clearly suggesting that the weakest points of the discontinuous 3DP gel networks were the semifused sites between the printed layers. This demonstrates that 3DP produced gels that will behave the same regardless of SFO concentration up to 40%. The fact that all the printed gels could only withstand a peak force of around 10 N shows the relative weakness of the 3DP network. The lowest value recorded for the cast gels was around 16 N for 40% SFO stabilised emulsion gels. The effects of delamination could be lessened by printing at higher temperatures to promote greater layer fu-

sion, although this could also lead to poorer shape fidelity as the printed solutions might not gel in time to hold their shape.

3.6. Post-printing oscillatory rheology

Oscillatory rheology also reinforced the trends observed in the TPA data, with 3DP κC emulsion gels displaying different microstructural characteristics to cast gels. Data from the amplitude sweeps, from which the LVER is determined is shown in Fig. 9.

The decreasing values for G' of the emulsion gels in both the 3DP and cast samples was in accordance with previous studies, whereby noninteracting filler particles reported lower G' values (Farjami & Madadlou, 2019). This trend held true across the 3DP and cast gels regardless of which emulsifier was present. WPI stabilised κC emulsion gels were found to have a slightly higher G', than those stabilised with T20, most probably owing to their reinforcement by the presence of salts. This is opposed to the TPA data from Fig. 8, which showed no statistically significant differences between hardness and Young's modulus for the two systems. This highlights the importance of multiple analysis techniques when it comes to complex systems such as emulsion gels. While T20 has been shown to also reinforce κC gel networks, this is generally observed at a far higher concentration (Fenton et al., 2021). However, another reason for the slight difference in G' is that as shown by the CLSM images in Fig. 7, WPI stabilised κC emulsion gels were not flocculated and therefore, while the data in Fig. 2 showed them to have a slightly larger droplet size, the fact that they remained dispersed meant that within the emulsion gels they would have had a smaller average droplet size (Chanamai & McClements, 2001). It has been shown that smaller oil droplet sizes give higher gel strength values in emulsion gels even when they're not bound to the gel matrix (Mcclements et al., 1993; Sala et al., 2009).

Furthermore, Fig. 9A and C reveal that the 3DP emulsion gels had a far smaller LVER compared to the cast gels and thus could be considered less resistant to shear strain. The oscillatory rheology data shows that the 3DP gels will break down faster than the cast gels. Based on this data and the data from the TPA, we hypothesise that it is once again due to delamination of the 3DP gels. However, unlike the TPA under the amplitude strain put out by the rheometer, the printed samples did not come close to matching the values observed for the cast gels at any concentration of SFO. The post-printing analysis by TPA oscillatory rheology shows that the WPI-stabilised κC 3DP emulsion gels form a slightly more robust network than the T20-stabilised ones. This is again suspected to be linked to either the differences in the effective oil droplet sizes caused by the flocculation in the T20 stabilised emulsion gel systems or the cations inherently present in the WPI.

4. Conclusions

This study shows that it is possible to produce emulsions with varying SFO concentrations, disperse 3% w/w κC in the water phase and print them to create emulsion gels. It has been shown that the emulsifying agent chosen can affect the emulsion gel structure, and can in turn, be affected by the gelling agent; with T20 emulsions gels flocculating, unlike emulsion gels stabilised with WPI. Several complex geometries were produced with a final print quality that was independent of the concentration of SFO, which was demonstrated by the μDSC data. While the SFO concentration affected the cast gels' mechanical properties, it has no appreciable effect on the 3DP gels. The current study therefore highlights the ability of 3DP to produce more complex food systems with multiple phases that can be tuned depending on the needs of the user. Future uses could involve release of lipophilic molecules or the addition of a dietarily relevant concentration of protein, to create a customisable total food source.

Supplementary materials

Supplementary material associated with this article can be found, in the online version, at doi:10.1016/j.fhfh.2021.100044.

References

Aaltonen, T., Kytö, E., Ylisjunttila-Huusko, S., & Outinen, M. (2020). Effect of the milk-based ash-protein ratio on the quality and acceptance of chocolate with a reduced sugar content. *International Dairy Journal, 105*, Article 104663.

Azam, R. S. M., Zhang, M., Bhandari, B., & Yang, C. (2018). Effect of different gums on features of 3D printed object based on vitamin-D enriched orange concentrate. *Food Biophysics, 13*(3), 250–262.

Beverung, C. J., Radke, C. J., & Blanch, H. W. (1999). Protein adsorption at the oil/water interface: Characterization of adsorption kinetics by dynamic interfacial tension measurements. *Biophysical Chemistry, 81*(1), 59–80.

Boland, A. B., Delahunty, C. M., & van Ruth, S. M. (2006). Influence of the texture of gelatin gels and pectin gels on strawberry flavour release and perception. *Food Chemistry, 96*(3), 452–460.

Buchanan, C., & Gardner, L. (2019). Metal 3D printing in construction: A review of methods, research, applications, opportunities and challenges. *Engineering Structures, 180*, 332–348.

Chanamai, R., & McClements, D. J. (2001). Depletion flocculation of beverage emulsions by gum Arabic and modified starch. *Journal of Food Science, 66*(3), 457–463.

Chanamai, R., & McClements, D. J. (2002). Comparison of gum Arabic, modified starch, and whey protein isolate as emulsifiers: Influence of pH, CaCl₂ and temperature. *Journal of Food Science, 67*(1), 120–125.

Chen, H., Xie, F., Chen, L., & Zheng, B. (2019). Effect of rheological properties of potato, rice and corn starches on their hot-extrusion 3D printing behaviors. *Journal of Food Engineering, 244*, 150–158.

Chen, J., Mu, T., Goffin, D., Blecker, C., Richard, G., Richel, A., et al. (2019). Application of soy protein isolate and hydrocolloids based mixtures as promising food material in 3D food printing. *Journal of Food Engineering*.

Chen, Z., Li, Z., Li, J., Liu, C., Lao, C., Fu, Y., et al. (2019). 3D printing of ceramics: A review. *Journal of the European Ceramic Society, 39*(4), 661–687.

Chimene, D., Lennox, K. K., Kaunas, R. R., & Gaharwar, A. K. (2016). Advanced bioinks for 3D printing: A materials science perspective. *Annals of biomedical Engineering, 44*(6), 2090–2102.

Daffner, K., Ong, L., Hanssen, E., Gras, S., & Mills, T. (2021). Characterising the influence of milk fat towards an application for extrusion-based 3D-printing of casein–whey protein suspensions via the pH–temperature-route. *Food Hydrocolloids*, Article 106642.

Dapčević Hadnađev, T., Dokić, P., Krstonošić, V., & Hadnađev, M (2013). Influence of oil phase concentration on droplet size distribution and stability of oil-in-water emulsions. *European Journal of Lipid Science and Technology, 115*(3), 313–321.

Diaz, J.V., Noort, M.W.J., & Van Bommel, K. J.C. (2017). Method for the production of an edible object by powder bed (3d) printing and food products obtainable therewith. In: Google Patents.

Diañez, I., Gallegos, C., Brito-de la Fuente, E., Martínez, I., Valencia, C., Sánchez, M. C., et al. (2019). 3D printing in situ gelification of κ-carrageenan solutions: Effect of printing variables on the rheological response. *Food Hydrocolloids, 87*, 321–330.

Dick, A., Bhandari, B., & Prakash, S. (2019). 3D printing of meat. *Meat Science, 153*, 35–44.

Du, J., Dai, H., Wang, H., Yu, Y., Zhu, H., Fu, Y., et al. (2021). Preparation of high thermal stability gelatin emulsion and its application in 3D printing. *Food Hydrocolloids, 113*, Article 106536.

Dun, H., Liang, H., Zhan, F., Wei, X., Chen, Y., Wan, J., et al. (2020). Influence of O/W emulsion on gelatinization and retrogradation properties of rice starch. *Food Hydrocolloids, 103*, Article 105652.

Farjami, T., & Madadlou, A. (2019). An overview on preparation of emulsion-filled gels and emulsion particulate gels. *Trends in Food Science & Technology, 86*, 85–94.

Fenton, T., Kanyuck, K., Mills, T., & Pelan, E. (2021). Formulation and characterisation of kappa-carrageenan gels with non-ionic surfactant for melting-triggered controlled release. *Carbohydrate Polymer Technologies and Applications, 2*, Article 100060.

Fontes-Candia, C., Ström, A., Lopez-Sanchez, P., López-Rubio, A., & Martínez-Sanz, M. (2020). Rheological and structural characterization of carrageenan emulsion gels. *Algal Research, 47*, Article 101873.

Gholamipour-Shirazi, A., Kamlow, M.-A., T Norton, I., & Mills, T (2020). How to formulate for structure and texture via medium of additive manufacturing-a review. *Foods, 9*(4), 497.

Gholamipour-Shirazi, A., Norton, I. T., & Mills, T. (2019). Designing hydrocolloid based food-ink formulations for extrusion 3D printing. *Food Hydrocolloids, 95*, 161–167.

Gibson, S. F., & Lanni, F. (1991). Experimental test of an analytical model of aberration in an oil-immersion objective lens used in three-dimensional light microscopy. *JOSA A, 8*(10), 1601–1613.

Goyanes, A., Scarpa, M., Kamlow, M., Gaisford, S., Basit, A. W., & Orlu, M. (2017). Patient acceptability of 3D printed medicines. *International Journal of Pharmaceutics, 530*(1-2), 71–78.

Gu, Y. S., Decker, E. A., & McClements, D. J. (2005). Influence of pH and carrageenan type on properties of β-lactoglobulin stabilized oil-in-water emulsions. *Food Hydrocolloids, 19*(1), 83–91.

Hemker, W. (1981). Associative structures of polyglycerol esters in food emulsions. *Journal of the American Oil Chemists' Society, 58*(2), 114–119.

Hermansson, A. M., Eriksson, E., & Jordansson, E. (1991). Effects of potassium, sodium and calcium on the microstructure and rheological behaviour of kappa-carrageenan gels. *Carbohydrate Polymers, 16*(3), 297–320.

Iglauer, S., Wu, Y., Shuler, P., Tang, Y., & Goddard III, W. A. (2011). Dilute iota-and kappa-Carrageenan solutions with high viscosities in high salinity brines. *Journal of Petroleum Science and Engineering, 75*(3-4), 304–311.

Iijima, M., Hatakeyama, T., Takahashi, M., & Hatakeyama, H. (2007). Effect of thermal history on kappa-carrageenan hydrogelation by differential scanning calorimetry. *Thermochimica Acta, 452*(1), 53–58.

Jones, D. S., Woolfson, A. D., & Brown, A. F. (1997). Textural, viscoelastic and mucoadhesive properties of pharmaceutical gels composed of cellulose polymers. *International Journal of Pharmaceutics, 151*(2), 223–233.

Jong, L. (2020). Poly(acrylic acid) grafted soy carbohydrate as thickener for waterborne paints. *Materials Today Communications, 23*, Article 100882.

Kamlow, M. A., Vadodaria, S., Gholamipour-Shirazi, A., Spyropoulos, F., & Mills, T. (2021). 3D printing of edible hydrogels containing thiamine and their comparison to cast gels. *Food Hydrocolloids, 116*, Article 106550.

Kelder, C., Bakker, A. D., Klein-Nulend, J., & Wismeijer, D. (2018). The 3D printing of calcium phosphate with K-carrageenan under conditions permitting the incorporation of biological components—a method. *Journal of Functional Biomaterials, 9*(4), 57.

Kenta, S., Raikos, V., Vagena, A., Sevastos, D., Kapolos, J., Koliadima, A., et al. (2013). Kinetic study of aggregation of milk protein and/or surfactant-stabilized oil-in-water emulsions by sedimentation field-flow fractionation. *Journal of Chromatography A, 1305*, 221–229.

Khalil, H., Lai, T., Tye, Y., Rizal, S., Chong, E., Yap, S., et al. (2018). A review of extractions of seaweed hydrocolloids: Properties and applications. *Express Polymer Letters, 12*(4).

Kim, K.-H., Gohtani, S., Matsuno, R., & Yamano, Y. (1999). Effects of oil droplet and agar concentration on gel strength and microstructure of o/w emulsion gel. *Journal of Texture Studies, 30*(3), 319–335.

Lanaro, M., Desselle, M. R., & Woodruff, M. A. (2019). 3D printing chocolate. In *Fundamentals of 3D Food Printing and Applications* (pp. 151–173).

Liu, Y., Yu, Y., Liu, C., Regenstein, J. M., Liu, X., & Zhou, P. (2019). Rheological and mechanical behavior of milk protein composite gel for extrusion-based 3D food printing. *LWT, 102*, 338–346.

Liu, Y., Zhang, W., Wang, K., Bao, Y., Regenstein, J. M., & Zhou, P. (2019). Fabrication of gel-like emulsions with whey protein isolate using microfluidization: Rheological properties and 3D printing performance. *Food and Bioprocess Technology, 12*(12), 1967–1979.

Liu, Z., Bhandari, B., Prakash, S., Mantihal, S., & Zhang, M. (2019). Linking rheology and printability of a multicomponent gel system of carrageenan-xanthan-starch in extrusion based additive manufacturing. *Food Hydrocolloids, 87*, 413–424.

Loizou, E., Weisser, J. T., Dundigalla, A., Porcar, L., Schmidt, G., & Wilker, J. J. (2006). Structural effects of crosslinking a biopolymer hydrogel derived from marine mussel adhesive protein. *Macromolecular Bioscience, 6*(9), 711–718.

Matsumura, Y., Kang, I. J., Sakamoto, H., Motoki, M., & Mori, T. (1993). Filler effects of oil droplets on the viscoelastic properties of emulsion gels. *Food Hydrocolloids, 7*(3), 227–240.

Mcclements, D. J., Monahan, F. J., & Kinsella, J. E. (1993). Effect of emulsion droplets on the rheology of whey protein isolate gels. *Journal of Texture Studies, 24*(4), 411–422.

Mizrahi, S. (2010). Syneresis in food gels and its implications for food quality. In *Chemical deterioration and Physical Instability of Food and Beverages* (pp. 324–348). Elsevier.

Norton, I. T., Morris, E. R., & Rees, D. A. (1984). Lyotropic effects of simple anions on the conformation and interactions of kappa-carrageenan. *Carbohydrate Research, 134*(1), 89–101.

Özcan, İ., Abacı, Ö., Uztan, A. H., Aksu, B., Boyacıoğlu, H., Güneri, T., et al. (2009). Enhanced topical delivery of terbinafine hydrochloride with chitosan hydrogels. *AAPS PharmSciTech, 10*(3), 1024–1031.

Padzi, M., Bazin, M. M., & Muhamad, W. (2017). Fatigue characteristics of 3D printed acrylonitrile butadiene styrene (ABS). *IOP Conference Series: Materials Science and Engineering, 269*, Article 012060.

Pal, R., & Rhodes, E. (1989). Viscosity/concentration relationships for emulsions. *Journal of Rheology, 33*(7), 1021–1045.

Pallottino, F., Hakola, L., Costa, C., Antonucci, F., Figorilli, S., Seisto, A., & Menesatti, P. (2016). Printing on food or food printing: A review. *Food and Bioprocess Technology, 9*(5), 725–733.

Rahim, T. N. A. T., Abdullah, A. M., & Md Akil, H. (2019). Recent developments in fused deposition modeling-based 3D printing of polymers and their composites. *Polymer Reviews, 59*(4), 589–624.

Sager, V. F., Munk, M. B., Hansen, M. S., Bredie, W. L. P., & Ahrné, L. (2021). Formulation of heat-induced whey protein gels for extrusion-based 3D printing. *Foods, 10*(1).

Saha, D., & Bhattacharya, S. (2010). Hydrocolloids as thickening and gelling agents in food: A critical review. *Journal of Food Science and Technology, 47*(6), 587–597.

Sala, G., de Wijk, R. A., van de Velde, F., & van Aken, G. A. (2008). Matrix properties affect the sensory perception of emulsion-filled gels. *Food Hydrocolloids, 22*(3), 353–363.

Sala, G., Van Aken, G. A., Stuart, M. A. C., & Van de Velde, F. (2007). Effect of droplet—Matrix interactions on large deformation properties of emulsion-filled gels. *Journal of Texture Studies, 38*(4), 511–535.

Sala, G., van Vliet, T., Cohen Stuart, M. A., Aken, G. A. v., & van de Velde, F. (2009). Deformation and fracture of emulsion-filled gels: Effect of oil content and deformation speed. *Food Hydrocolloids, 23*(5), 1381–1393.

Serizawa, R., Shitara, M., Gong, J., Makino, M., Kabir, M. H., & Furukawa, H. (2014). 3D jet printer of edible gels for food creation. In *Behavior and Mechanics of Multifunctional Materials and Composites 2014: 9058* (p. 90580A). International Society for Optics and Photonics.

Severini, C., Derossi, A., Ricci, I., Caporizzi, R., & Fiore, A. (2018). Printing a blend of fruit and vegetables. New advances on critical variables and shelf life of 3D edible objects. *Journal of Food Engineering, 220*, 89–100.

Singh, H., Tamehana, M., Hemar, Y., & Munro, P. A. (2003). Interfacial compositions, microstructure and stability of oil-in-water emulsions formed with mixtures of milk proteins and κ-carrageenan: 2. Whey protein isolate (WPI). *Food Hydrocolloids, 17*(4), 549–561.

Singla, V., Saini, S., Joshi, B., & Rana, A. (2012). Emulgel: A new platform for topical drug delivery. *International Journal of Pharma and Bio Sciences, 3*(1), 485–498.

Snoeren, T. H. M., & Payens, T. A. J. (1976). On the sol-gel transition in solutions of Kappa-carrageenan. *Biochimica et Biophysica Acta (BBA) - General Subjects, 437*(1), 264–272.

Sun, J., Zhou, W., Huang, D., Fuh, J. Y. H., Hong, G. S. J. F., & Technology, B. (2015). An overview of 3D printing technologies for food fabrication. 8(8), 1605-1615.

Teo, A., Goh, K. K. T., Wen, J., Oey, I., Ko, S., Kwak, H. S., et al. (2016). Physicochemical properties of whey protein, lactoferrin and Tween 20 stabilised nanoemulsions: Effect of temperature, pH and salt. *Food Chemistry, 197*, 297–306.

Thakur, G., Naqvi, M. A., Rousseau, D., Pal, K., Mitra, A., & Basak, A. (2012). Gelatin-based emulsion gels for diffusion-controlled release applications. *Journal of Biomaterials Science, Polymer Edition, 23*(5), 645–661.

Ubbink, J., Burbidge, A., & Mezzenga, R. (2008). Food structure and functionality: A soft matter perspective. *Soft Matter, 4*(8), 1569–1581.

Vadodaria, S. S., He, Y., Mills, T., & Wildman, R. (2020). Fabrication of surfactant-polyelectrolyte complex using valvejet 3D printing-aided colloidal self assembly. *Colloids and Surfaces A: Physicochemical and Engineering Aspects, 600*, Article 124914.

Warner, E. L., Norton, I. T., & Mills, T. B. (2019). Comparing the viscoelastic properties of gelatin and different concentrations of kappa-carrageenan mixtures for additive manufacturing applications. *Journal of Food Engineering, 246*, 58–66.

Wilde, P., Mackie, A., Husband, F., Gunning, P., & Morris, V. (2004). Proteins and emulsifiers at liquid interfaces. *Advances in Colloid and Interface Science, 108-109*, 63–71.

Williams, P., Clegg, S., Langdon, M., Nishinari, K., & Piculell, L. (1993). Investigation of the gelation mechanism in. kappa.-carrageenan/konjac mannan mixtures using differential scanning calorimetry and electron spin resonance spectroscopy. *Macromolecules, 26*(20), 5441–5446.

Wu, M. H., Yan, H. H., Chen, Z. Q., & He, M. (2017). Effects of emulsifier type and environmental stress on the stability of curcumin emulsion. *Journal of Dispersion Science and Technology, 38*(10), 1375–1380.

Wu, Y., Petrochenko, P., Chen, L., Wong, S. Y., Absar, M., Choi, S., et al. (2016). Core size determination and structural characterization of intravenous iron complexes by cryogenic transmission electron microscopy. *International Journal of Pharmaceutics, 505*(1), 167–174.

Yang, F., Zhang, M., Bhandari, B., & Liu, Y. (2018). Investigation on lemon juice gel as food material for 3D printing and optimization of printing parameters. *LWT, 87*, 67–76.

Yang, F., Zhang, M., Prakash, S., & Liu, Y. (2018). Physical properties of 3D printed baking dough as affected by different compositions. *Innovative Food Science & Emerging Technologies, 49*, 202–210.